IEEE Access
Multidisciplinary | Rapid Review | Open Access Journal

Received March 29, 2021, accepted April 7, 2021, date of publication April 14, 2021, date of current version April 26, 2021.

Digital Object Identifier 10.1109/ACCESS.2021.3073108

A Novel Hybrid Control Strategy for the Energy Storage Modular Multilevel Converters

QINGQING YUAN, FENGNIAN YANG, AN LI, AND TING MA
Department of Electrical Engineering, University of Shanghai for Science and Technology, Shanghai 200093, China
Corresponding author: Qingqing Yuan (yuanqq@usst.edu.cn)

This work was supported in part by the Shanghai Sailing Program under Grant 18YF1418300.

ABSTRACT In this paper, a novel hybrid control strategy has been proposed for the energy storage modular multilevel converters (ESMMC) to realize a nice current performance and ensure the state of change (SOC) of batteries to be balanced. Firstly, traditional proportional integral (PI) control was used to get the circulating current reference; then an improved model predictive control (MPC) method with the weighting factors being online tuned has been designed to obtain the accessing numbers of the submodules in each phase. Lastly, the conventional sorting method for the SOC balancing was given. Experimental comparisons indicate that this proposed novel control strategy can not only ensure a nice current control performance, but also effectively suppress the circulating current component, and it can save over 39.42% execution time in contrast with the traditional PI method, which is feasible for the digital implementation.

INDEX TERMS Energy storage modular multilevel converter (ESMMC), hybrid control, improved model predictive control (MPC), weighting factors online tuning.

NOMENCLATURE

ESMMC	Energy storage modular multilevel converter
SOC	State of charge
PI	Proportional integral
MPC	Model predictive control
MMC	Modular multilevel converter
HVDC	High voltage direct current
ESSM	Energy storage submodule

I. INTRODUCTION

Nowadays, modular multilevel converters (MMCs) have a rapid development in the high-voltage and high-power applications, e.g., high voltage direct current (HVDC) transmission, reactive compensation, grid integration of renewable energy generation and so on, for their high efficiency and low output harmonic distortion [1]–[3]. On the other hand, large-scale renewable energy generation system usually needs energy storage devices to absorb or release the power and effectively reduce the impact resulted from converters' output fluctuation on the power with the considerations of the intermittent and uncertain characteristics of the renewable energies [4]–[8]. In traditional energy storage systems, the energy storage batteries were usually connected to the grid through former boost converter and later inverter circuits which reduced the system efficiency and reliability [9]. If the energy storage system is combined with the grid connected converters themselves, then a decentralized access would be realized, which is suitable for the large-scale renewable energy generation systems, and the studies on which will have certain research significance [10]–[13].

In terms of the MMC-based energy storage system, related research has become one of the hot spots. In [14], a SOC balancing algorithm was studied under different operating modes to eliminate the low-frequency components in the output currents, and the unbalanced grid conditions were also taken into account. Reference [11] proposed a novel configuration, in which the batteries and supercapacitors were distributed into the upper and lower arms, which could realize a fully decoupled power control between the grid and hybrid storage systems. In [15], different control modes adopted for the hybrid energy storage systems were given and compared. In [16], the SOC of each energy storage battery has been balanced by adjusting the modulation of submodules. In [17], for the SOC balancing issues, the influences of different circulating current components have been analysed in detail, while in [18], the performance availability and flexibility of an energy storage-based MMC was given by theoretical and experimental discussion.

The associate editor coordinating the review of this manuscript and approving it for publication was Yijie Wang.

MPC has gradually expanding applications in the field of power electronical systems due to its outstanding advantages in dealing with the problems of nonlinear system and the complex constraints issues [3], [19], 21]. In [21], the traditional finite control set MPC (FCS-MPC) strategy has been used for the MMC system, which could eliminate the circulating current components and regulate the arm voltages, ac-side currents, the computational complexity was the one of the main factors affecting performance. In [22], well-reported experimental comparison between MPC and traditional PI strategies were given. To improve the execution efficiency, a novel step-by-step rolling optimization method was proposed in [23], but it didn't involve the design of weighting factors. A novel sliding-discrete-control-set modulated MPC method was proposed for MMC in [24] to simplify the computational complexity, but this method did not involve the consideration of weight factors and each submodular obtained a fixed switching frequency. In [25], an improved MPC integrated with PI was proposed to reduce the computational complexity.

In this paper, a novel hybrid control strategy has been proposed for the ESMMCs on the basis of existing research. This hybrid control involves three parts: a traditional PI control, an improved MPC strategy and a conventional SOC balancing method. The control targets include ac-side current tracking and the circulating current suppression. In detail, PI control is used to get the circulating current references including dc and ac components; the improved MPC strategy is designed to obtain the accessing numbers of the submodules in each phase, and an online tuning method has also been proposed to improve the control performance; and the conventional sorting method is used for the SOC balancing.

The paper is organized as follows. In Section II, the principle and the discrete mathematical models of this studied ESMMC is given. Section III presents the hybrid control strategy in details and the online tuning method for the weighting factors is also introduced in terms of realization process. The effectiveness of this designed strategy is discussed in Section IV in terms of contrast experimental results. Finally, Section V gives the conclusion.

II. PRINCIPLE AND MATHEMATICAL MODELS OF ESMMC

The three-phase ESMMC shown in Figure 1 is taken as the research object, in which each phase contains upper and lower bridge arms and each arm is composed of N energy storage submodules (ESSMs) and one bridge arm inductance, and capacitors C_1 and C_2 are the dc-link capacitors. Each ESSM consists of two switching devices T_1 and T_2, two diodes D_1 and D_2, capacitor C_0 ($C_0 = 1500\mu$F, the design consideration is in the Appendix) and the energy storage battery Bat.

Take one phase as an example to establish the mathematical models, then the simplified circuit of j-phase (j = a, b, c) is shown in Figure 2, in which each ESSM is equivalent to a controlled voltage source. Where, u_{pj} represents the upper bridge arm voltage of j-phase, which equals to the sum of voltages of the accessing submodules in the upper bridge arm; while u_{nj} represents the lower bridge arm voltage and equals to the sum of voltages of the accessing submodules in the lower bridge arm. i_{pj} and i_{nj} are the upper and lower bridge arm current components respectively. U_{dc} is the dc-link voltage while i_{dc} is the dc-link current; u_j and i_j stand for the output voltage and current components in the ac-side respectively, while u_{sj} is the grid voltage. L_a represents the bridge arm filter inductance ($L_a = 5$mH, the design consideration is in the Appendix) and L_s is the filter inductance in the ac-side.

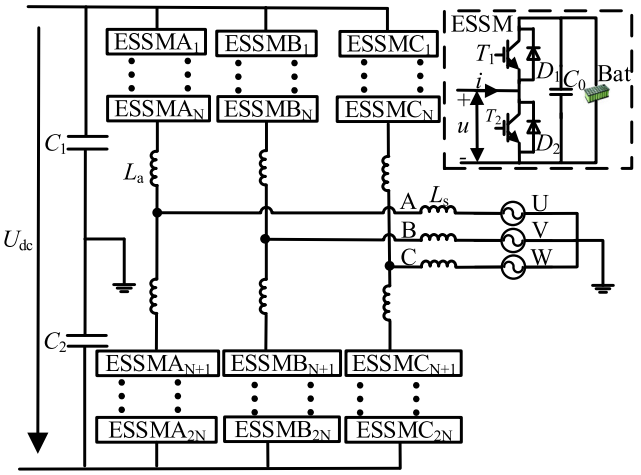

FIGURE 1. Topology of the studied three-phase ESMMC.

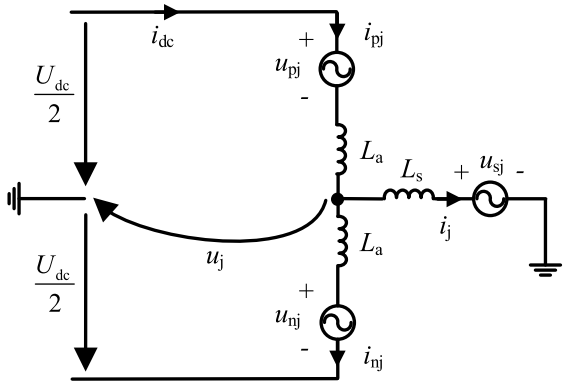

FIGURE 2. Simplified circuit of j-phase.

Defining S_{rjk} as the switching function of the k^{th} ESSM in j-phase and r-bridge (r = p or n, referring the upper or lower bridge arm respectively), and it is described as

$$S_{rjk} = \begin{cases} 1, & T_1 \text{is ON, } T_2 \text{ is OFF} \\ 0, & T_1 \text{is OFF, } T_2 \text{ is ON} \end{cases} \tag{1}$$

Considering that there are N working ESSMs in each phase, the sum of the switching functions for each phase is N, which means

$$\sum_{k=1}^{N} S_{pjk} + \sum_{k=1}^{N} S_{njk} = N \tag{2}$$

And the voltage of each ESSM can be written as

$$u_{rjk} = S_{rjk} \cdot U_{SM} \tag{3}$$

Voltages of the upper and lower bridge arms can be derived as

$$\begin{cases} u_{\mathrm{pj}} = \sum_{k=1}^{N} S_{\mathrm{pjk}} \cdot U_{\mathrm{SM}} \\ u_{\mathrm{nj}} = \sum_{k=1}^{N} S_{\mathrm{njk}} \cdot U_{\mathrm{SM}} \end{cases} \tag{4}$$

According to Kirchhoff's voltage law and Kirchhoff's current law, following voltage and current equations can be derived

$$\begin{cases} \frac{U_{\mathrm{dc}}}{2} = u_{\mathrm{pj}} + L_{\mathrm{a}} \frac{di_{\mathrm{pj}}}{dt} + L_{\mathrm{s}} \frac{di_{\mathrm{j}}}{dt} + u_{\mathrm{sj}} \\ \frac{U_{\mathrm{dc}}}{2} = u_{\mathrm{nj}} + L_{\mathrm{a}} \frac{di_{\mathrm{nj}}}{dt} - L_{\mathrm{s}} \frac{di_{\mathrm{j}}}{dt} - u_{\mathrm{sj}} \end{cases} \tag{5}$$

$$i_{\mathrm{j}} = i_{\mathrm{pj}} - i_{\mathrm{nj}} \tag{6}$$

$$u_{\mathrm{j}} = L_{\mathrm{s}} \frac{di_{\mathrm{j}}}{dt} + u_{\mathrm{sj}} \tag{7}$$

With the combination of equations (5)-(7), the output voltage u_{j} can be derived as following (the inductive voltages of the bridge arm are ignored, which means $L_{\mathrm{a}} \frac{di_{\mathrm{pj}}}{dt} = L_{\mathrm{a}} \frac{di_{\mathrm{nj}}}{dt} = 0$).

$$u_{\mathrm{j}} = \frac{u_{\mathrm{nj}} - u_{\mathrm{pj}}}{2} \tag{8}$$

On the other hand, making a definition of bridge arm circulating current component flowing the upper and lower bridge arms as [26].

$$i_{\mathrm{cirj}} = \frac{i_{\mathrm{pj}} + i_{\mathrm{nj}}}{2} \tag{9}$$

Then, the upper and lower bridge arm current components i_{pj} and i_{nj} can be obtained by equations (6) and (9).

$$\begin{cases} i_{\mathrm{pj}} = i_{\mathrm{cirj}} + \frac{i_{\mathrm{j}}}{2} \\ i_{\mathrm{nj}} = i_{\mathrm{cirj}} - \frac{i_{\mathrm{j}}}{2} \end{cases} \tag{10}$$

From equation (10), it can be seen that for the bridge arm current components i_{pj} and i_{nj}, there not only has ac side current component i_{j} and also has the internal circulating current component i_{cirj}.

Considering that there is no even harmonic existing in the ESMMC, so the circulating current component, only includes the DC and fundamental components, and can be written as [26]

$$i_{\mathrm{cirj}} = i_{\mathrm{cirj\_dc}} + i_{\mathrm{cirj\_ac}} \tag{11}$$

where, $i_{\mathrm{cirj\_dc}}$ is the DC circulating current component and $i_{\mathrm{cirj\_ac}}$ is the fundamental circulating current component.

III. HYBRID CONTROL STRATEGY

Considering the large number of switching states for the ESMMC and the relatively complicated control, a novel hybrid control strategy, including normal PI control, model predictive control (MPC) and the SOC balancing, is proposed in this paper.

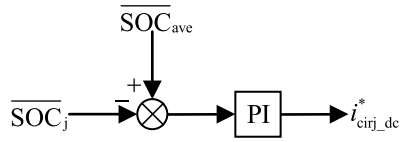

FIGURE 3. SOC control structure between three phases.

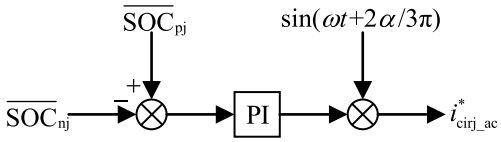

FIGURE 4. SOC control structure within each phase.

A. PI CONTROL PART

For the SOCs between three phases, the control structure is shown in Figure 3 and the control output corresponds to given value of the DC circulating current component $i^*_{\mathrm{cirj\_dc}}$.

For the SOCs within each phase, the control structure is shown in Figure 4(when $\mathrm{j} = \mathrm{a}, \alpha = 0; \mathrm{j} = \mathrm{b}, \alpha = -1$ and $\mathrm{j} = \mathrm{c}, \alpha = 1$), the control output corresponds to the given value of the fundamental circulation component $\mathrm{i}^*_{\mathrm{cirj\_ac}}$.

In which, $\overline{\mathrm{SOC}}_{\mathrm{j}}$ is the average SOC of the j-phase batteries; $\overline{\mathrm{SOC}}_{\mathrm{pj}}$ is the average SOC of the batteries in the upper bridge arm of j-phase; $\overline{\mathrm{SOC}}_{\mathrm{nj}}$ is the average SOC of the batteries in the lower bridge arm of j-phase; $\overline{\mathrm{SOC}}_{\mathrm{ave}}$ represents the average SOC of all the batteries in the three-phase arms.

Thus, the overall reference value of circulating current $\mathrm{i}^*_{\mathrm{cirj}}$ can be obtained as

$$i^*_{\mathrm{cirj}} = i^*_{\mathrm{cirj\_dc}} + i^*_{\mathrm{cirj\_ac}} \tag{12}$$

B. MPC PART

1) OBJECTIVE FUNCTION

Firstly, according to equations (5), (6) and (9), the predicted current in ac-side and circulating current components at $(k+1)^{\mathrm{th}}$ can be derived as

$$\begin{cases} i^{\mathrm{p}}_{\mathrm{j}}(k+1) = \frac{T_{\mathrm{s}}}{L_{\mathrm{s}} + L_{\mathrm{a}}/2} \cdot \left(\frac{u_{\mathrm{nj}}(k) - u_{\mathrm{pj}}(k)}{2} - u_{\mathrm{sj}}(k) \right) + i_{\mathrm{j}}(k) \\ i^{\mathrm{p}}_{\mathrm{cirj}}(k+1) = \frac{T_{\mathrm{s}}}{2L_{\mathrm{a}}} \cdot (U_{\mathrm{dc}} - (u_{\mathrm{pj}}(k) + u_{\mathrm{nj}}(k))) + i_{\mathrm{cirj}}(k) \end{cases} \tag{13}$$

In which, bridge arm voltages of j-phase at k^{th} sampling time can be obtained by the switching states and the battery voltage U_{SM}.

$$\begin{cases} u_{\mathrm{pj}}(k) = \sum_{i=1}^{N} U_{\mathrm{SM}} \cdot S_{\mathrm{pjk}}(k) \\ u_{\mathrm{nj}}(k) = \sum_{i=1}^{N} U_{\mathrm{SM}} \cdot S_{\mathrm{njk}}(k) \end{cases} \tag{14}$$

The objective function consists of two parts: ac-side current trajectory and the circulating current suppression, which is displayed in equation (15).

$$g = \lambda_1 \left| i^*_{\mathrm{j}}(k+1) - i^{\mathrm{p}}_{\mathrm{j}}(k+1) \right| + \lambda_2 \left| i^*_{\mathrm{cirj}}(k+1) - i^{\mathrm{p}}_{\mathrm{cirj}}(k+1) \right| \tag{15}$$

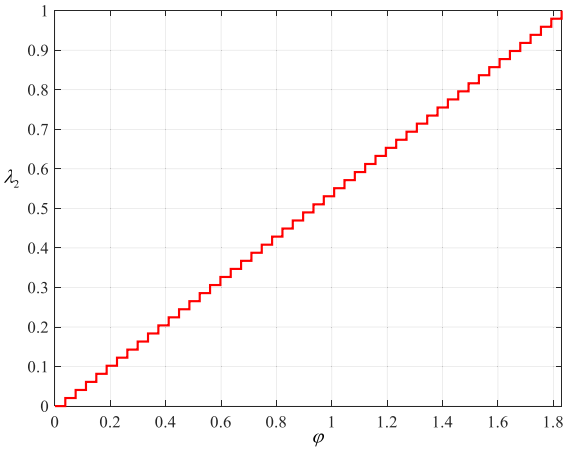

FIGURE 5. Off-line preparation of weighting factor λ_2.

where, λ_1 and λ_2 are the weighting factors, $i_j^*(k+1)$ and $i_{cirj}^*(k+1)$ are the expected ac-side and circulating current components at $(k+1)^{th}$ sampling period.

2) ONLINE TUNING FOR THE WEIGHTING FACTORS

In order to improve the control performance, an online tuning method for the weighting factors has been proposed in this paper. Firstly, setting $\lambda_1 = 1$ because the ac-side current trajectory has a highest priority, then an online tuning method based on the experiences and the detailed processes are summarized as following.

a: OFF-LINE PREPARATIONS

The second item in equation (15) is separately defined as an objective function (as shown in equation (16)).

$$g_2 = \left| i_{cirj}^*(k+1) - i_{cirj}^p(k+1) \right| \tag{16}$$

Step 1: Sufficient $\lambda_2 \in (0,1)$ were taken as the sampled data to get plentiful different g_2.

Step 2: Defining an acceptable error φ, and making a division of the error band to m bands, and the corresponding weighting factor λ_2 is also divided into m bands as $\lambda_2 = u/m$ ($u \in \{1,2,3,\ldots, m\}$), the detailed correspondence can be systematized into as

$$\begin{aligned} (0, \varphi) &\Rightarrow \lambda_2 = \frac{1}{m} \\ (\varphi, 2\varphi) &\Rightarrow \lambda_2 = \frac{2}{m} \\ (2\varphi, 3\varphi) &\Rightarrow \lambda_2 = \frac{3}{m} \\ &\cdots \\ ((m-1)\varphi, m\varphi) &\Rightarrow \lambda_2 = \frac{u}{m} \\ (u &\in \{1, 2, 3, \ldots, m\}) \end{aligned} \tag{17}$$

To be specific, the sub-target g_2 is in the range of 0 to 1.83 with sufficient $\lambda_2 \in (0,1)$ being taken as the sampled data, and m is set as 50, the acceptable error $\varphi = 1.83/50$, then the corresponding weighting factor λ_2 is divided into 50 bands as $\lambda_2 = u/50$ ($u \in \{1,2,3,\ldots,50\}$), the corresponding relationship between λ_2 and φ is shown in Figure 5.

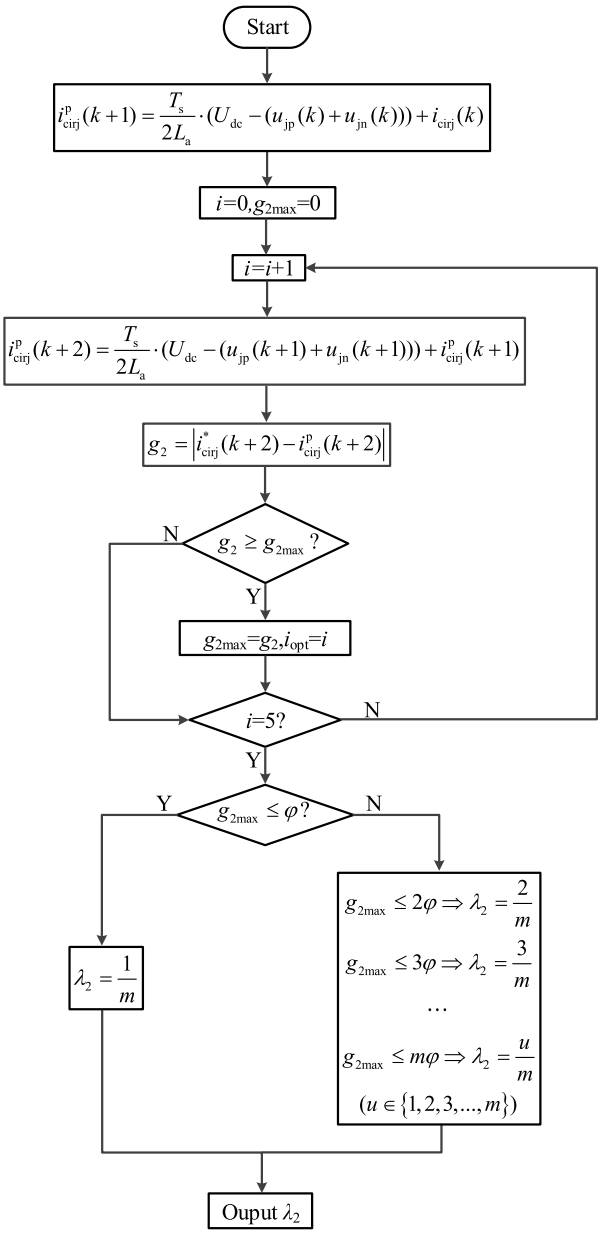

FIGURE 6. Online optimization of the weighting factor.

b: ONLINE TUNING

Step 1: Before the rolling optimization of equation (15) during each sampling period, g_{2max} from equation (16) should be firstly obtained.

Step 2: Judging the range of g_{2max}, and the corresponding weighting factor λ_2 can be get according to equation (17).

Step 3: Substituting the real-timely obtained λ_2 into equation (15) to carry out the rolling optimization of g and get the optimized g_{min}.

The detailed online tuning process of the weighting factor λ_2 is shown in Figure 6, and this online tuning method can

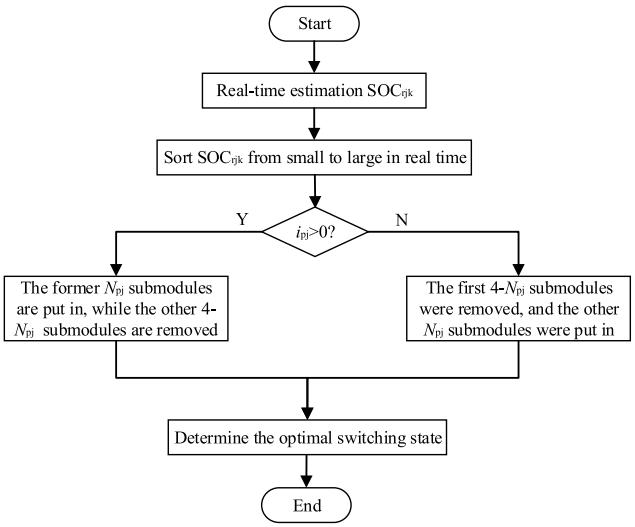

FIGURE 7. Sorting method for the SOC balancing.

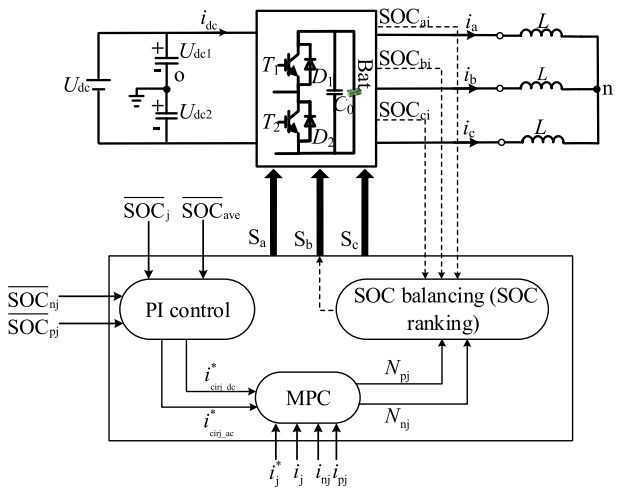

FIGURE 8. The Control diagram of this proposed novel hybrid control.

ensure the ac-side current trajectory to be taken as the primary control target and the subobjective g_2 can be chosen to the setting error band to the maximum extent.

On the other hand, a simple compensation with one step forward prediction has also been studied because of the inherent time delay problem of MPCC. In practical applications, the current prediction value at $k+1$ sampling time is used as the sampling value for the next cycle of current prediction calculations, and $i(k+2)$ is substituted into the objective function (equation (19)) for optimization.

C. SORTING METHOD FOR THE SOC BALANCING

After the confirmation of the accessing number of the submodules, a conventional SOC soring method is opted to verify the effectiveness of the proposed hybrid control algorithm, especially the improved MPC strategy, the corresponding implementation process is shown in Figure 7, in which N_{pj} is the accessing number of submodules in the upper bridge

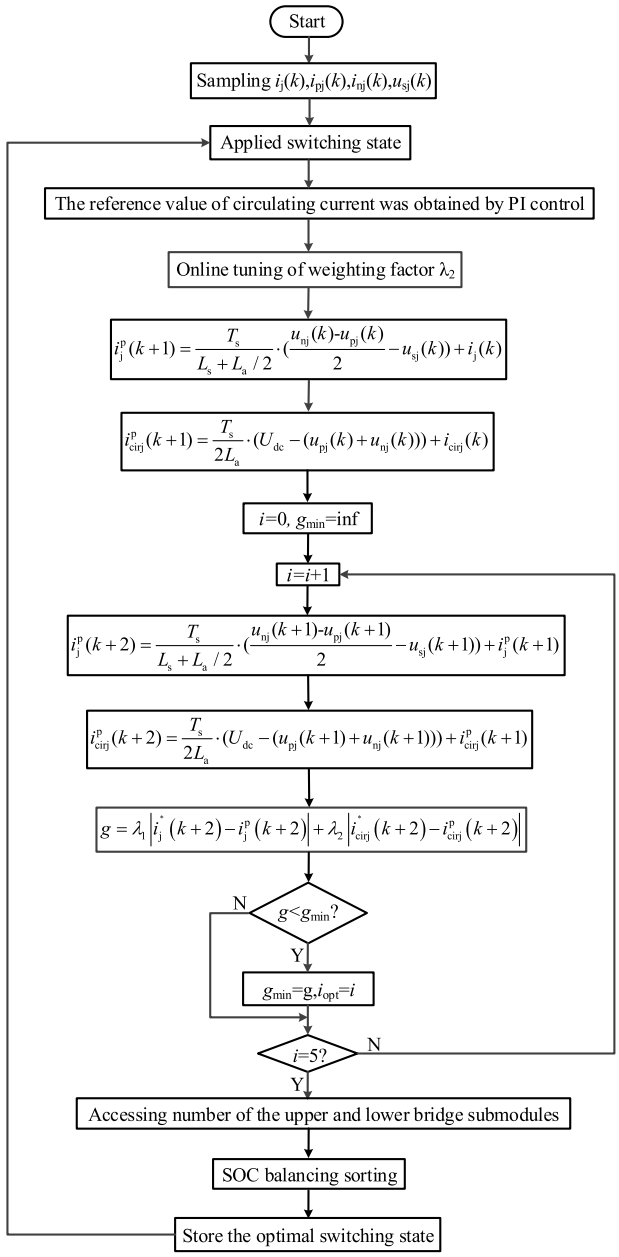

FIGURE 9. Flow chart of the novel hybrid control strategy.

arm of j-phase, N_{nj} is the accessing number of submodules in the lower bridge arm of j-phase, and SOC_{rjk} is the SOC value of the k^{th} submodule in r-bridge j-phase.

Control diagram and flow chart of the novel hybrid control strategy are shown in Figure 8 and Figure 9 respectively.

IV. EXPERIMENTAL RESULTS

An experimental platform for this studied five-level ESMMC, which is shown in Figure 10, has been established to make verifications and the detailed parameters are listed in Table 1.

For the online tuning of weighting factor λ_2, the real-time adjusting process within 0.01s is shown in Figure 11.

The static phase and line voltage waveforms at the moment when the modulation index $M = 0.9$ are shown

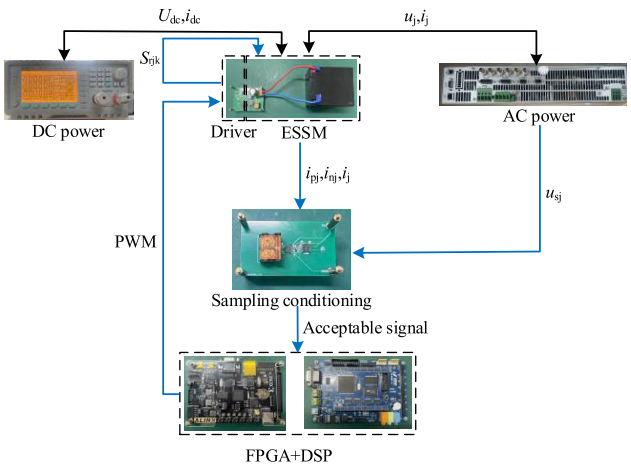

FIGURE 10. Structure of the experimental platform.

TABLE 1. Detailed parameters of this studied five-level ESMMC.

Parameter name	Parameter value
Dc-link voltage U_{dc}	800V
Dc-link current I_{dc}	12.5A
System Power factor	cos φ = 0.95
Amplitude of the output phase voltage in ac-side u_j	400V
Battery capacity	100Ah
Amplitude of the reference current	16A
Bridge arm inductance L_a	5mH
ac-side inductance L_s	5mH
Fundamental frequency	50Hz
Sampling frequency	10kHz

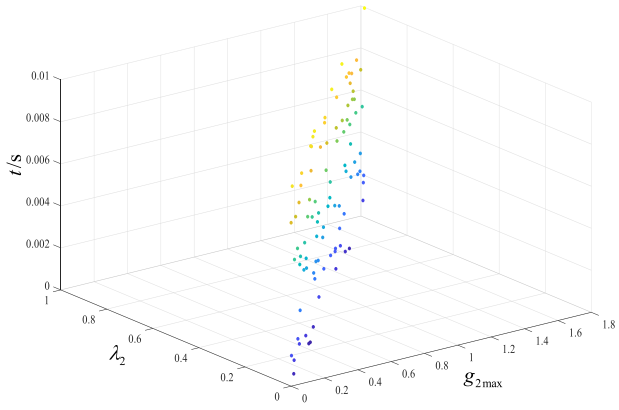

FIGURE 11. Real-time adjusting process of weighting factor λ_2.

in Figure 12. The ac-side reference and actual current components in a-phase are displayed in Figure 13, and the harmonic distortion of the actual current is analyzed in Figure 14.

Obviously, these responses show that this proposed novel control strategy is reasonable and the static effect is acceptable.

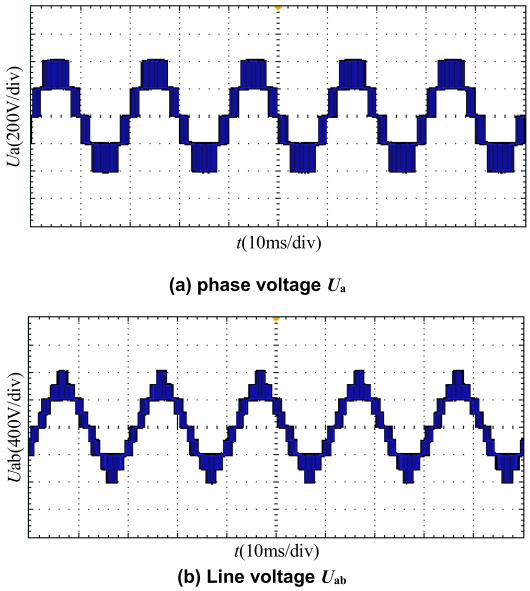

FIGURE 12. Static phase and line voltage waveforms.

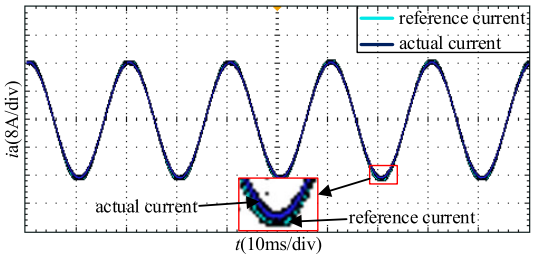

FIGURE 13. Reference and actual current components in a-phase.

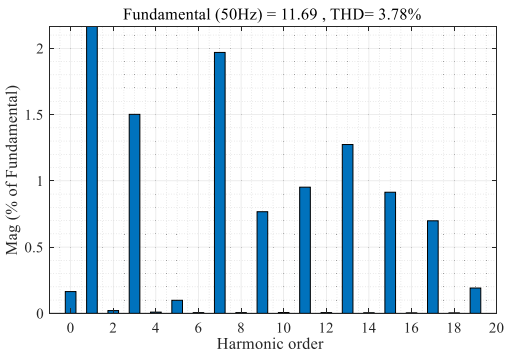

FIGURE 14. Harmonic distortion of the actual current in a-phase.

For the circulating current suppression, the amplitude is limited to ±0.9A as shown in Figure 15, by which the effectiveness of the hybrid control strategy is verified in further.

In terms of dynamic responses, when the reference current's amplitude changes from 16A to 10A, the corresponding responses of the ac-side current and circulation component are shown in Figure 16(a) and (b), which shows that this studied novel control strategy has a nice dynamic response performance.

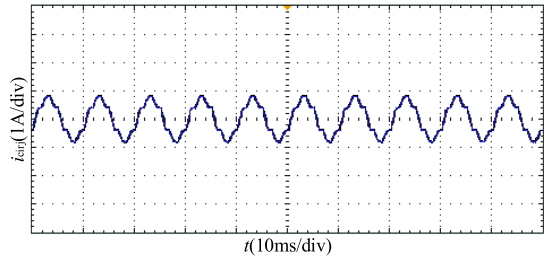

FIGURE 15. Circulating current.

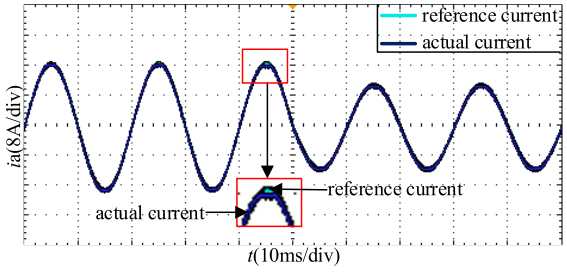

(a) Reference and actual current components in a-phase

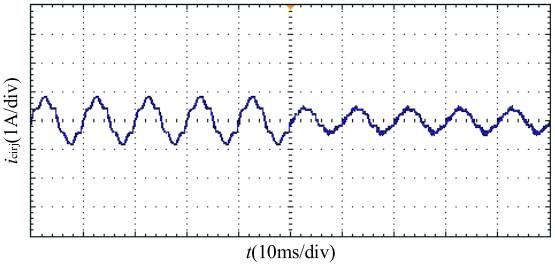

(b) Dynamic circulating current

FIGURE 16. Dynamic current responses.

In order to verify the effectiveness of SOC balancing control, small SOC deviations were initially set considering of the inertia constant issue. The SOC balancing responses within and between bridge arms, interphase are shown in Figure 17, in which, SOC reaches balancing at about 0.5s, and the response speed is relatively acceptable.

In order to compare with different control strategies (traditional PI method; off-line weighting factors and without delay compensation; off-line weighing factors with delay compensation; this novel hybrid control method), the harmonic distortion of the ac-side current under different modulation ($M \in [0.5\ 0.9]$) indexes are compared in Figure 18, which can show the superiority of this novel control strategy. Accordingly, the comparisons of SOC balancing rates are displayed in Figure 19.

It can be seen that the SOC balancing time increases with the increase of modulation index and the control strategy proposed in this paper maintains a faster balancing rate under different modulation indexes.

Considering of the feasibility of digital implementation, the execution efficiency of different method is also compared as listed in Table 2. Compared with traditional PI method,

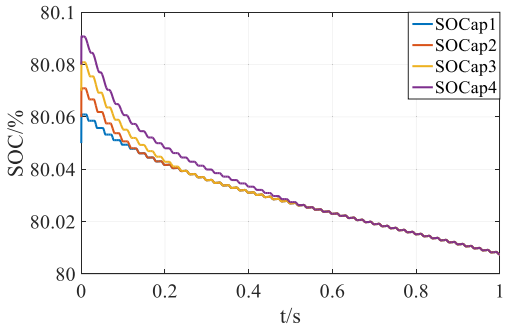

(a) SOC balancing within bridge arms in the upper bridge of a-phase

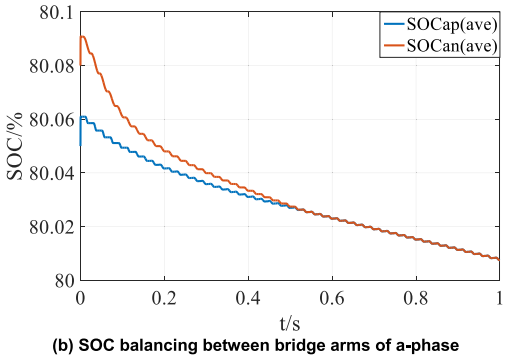

(b) SOC balancing between bridge arms of a-phase

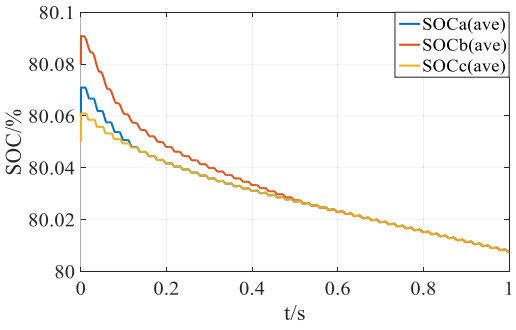

(c) Interphase SOC balancing

FIGURE 17. Changing trends of SOC in different submodules.

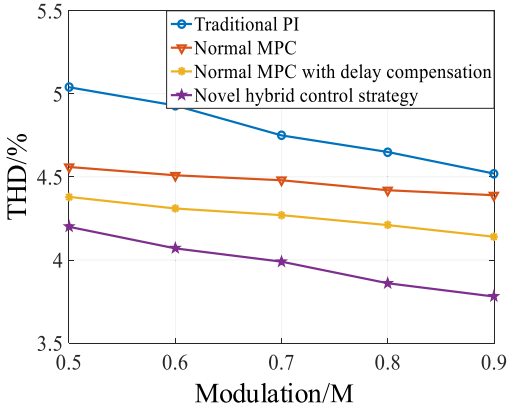

FIGURE 18. Harmonic distortion comparisons with different control strategies.

normal MPC method can save about 54.66% and about 46.31% with a delay compensation, and this new control

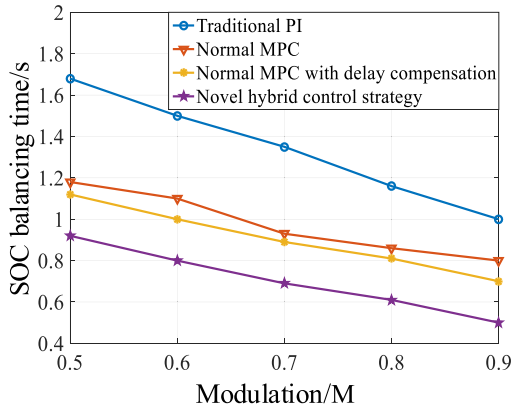

FIGURE 19. Comparisons of the SOC balancing time with different control strategies.

TABLE 2. Execution efficiency of different control strategies.

Method	Execution time (μs)	Save time (compared to PI) (%)
Traditional PI	82.7	
Normal MPC	37.5	54.66
Normal MPC with delay compensation	44.4	46.31
Novel hybrid control strategy	50.1	39.42

strategy can save about 39.42%, which is convenient for digital implementation.

V. CONCLUSION

In order to maintain a nice control performance for the five-level energy storage modular multilevel converter, a novel hybrid control strategy has been studied in detail. With the traditional PI control, the circulating current reference was obtained, which then was taken with the rolling optimization of an improved MPC strategy, along with the ac-side current tracking control. Then with the gotten accessing numbers of submodules in each phase, the conventional sorting method for the SOC balancing was used to realize the SOC balancing. On the other hand, an online tuning method for the weighing factors in MPC strategy was designed to improve the execution efficiency.

The effectiveness of this novel hybrid control strategy is verified by experimental comparisons, which can save 39.42% execution time of the traditional PI method and has better superiority in current control, circulating current suppression and SOC balancing rates. In the future, the online tuning method of weighting factor would be perfected further to improve performance when multi-objective constrains are considered.

APPENDIX

$$C_{\mathrm{o}} = \frac{U_{\mathrm{dc}} I_{\mathrm{j}}}{4\omega N \varepsilon U_{\mathrm{CO}}^2}\left[1 - \frac{m^2(1+\cos^2\varphi_{\mathrm{j}})}{3}\right] \le \frac{U_{\mathrm{dc}} I_{\mathrm{j}}}{4\omega N \varepsilon U_{\mathrm{CO}}^2} \tag{A.1}$$

where, I_{j} is amplitude of the reference output phase current ($I_{\mathrm{j}} = 16\mathrm{A}$); ω is the angular frequency of the output fundamental component ($\omega = 2\times\pi\times50$); ε is the ripple coefficient of the capacitor voltage, and in this paper, ε is setting as 5%; U_{CO} is the capacitor voltage ($U_{\mathrm{CO}} = 200\mathrm{V}$); m is the modulation index.

In order to ensure the stable operation capacitance C_{o} is designed by the maximum value calculated by equation (A.1), that is

$$C_{\mathrm{o}} = \frac{U_{\mathrm{dc}} I_{\mathrm{j}}}{4\omega N \varepsilon U_{C_o}^2} = \frac{800\times16}{4\times314\times4\times5\%\times200^2} = 1273.88\mu\mathrm{F} \tag{A.2}$$

According to the parameters of the actual aluminum electrolytic capacitor, a 1500V/400A capacitor was selected as C_{o}.

$$L_{\mathrm{a}} = \frac{1}{8\omega^2 C_{\mathrm{o}} U_{\mathrm{CO}}}\left(\frac{P_{\mathrm{s}}}{3I_{\mathrm{cirj}}} + U_{\mathrm{dc}}\right) \tag{A.3}$$

where, Ps is the Apparent Power and I_{cirj} is the peak value of the bridge arm circulating current.

The RMS value the reference output phase current I_{jN} is $16/\sqrt{2} = 11\mathrm{A}$, and the I_{cirj} could be derived as

$$I_{\mathrm{cirj}} = 0.35\times\left(\frac{I_{\mathrm{jN}}}{2} + \frac{I_{\mathrm{dc}}}{3}\right) = 0.35\times\left(\frac{11}{2} + \frac{12.5}{3}\right) = 9.67\mathrm{A} \tag{A.4}$$

Then, L_{a} could be derived as

$$L_{\mathrm{a}} = \frac{1}{8\times314^2\times1500\times10^{-6}\times200}\left(\frac{\frac{800\times12.5}{0.95}}{3\times9.67} + 800\right) = 5\mathrm{mH} \tag{A.5}$$

REFERENCES

[1] K. Ji, S. Liu, H. Pang, J. Yang, Z. Xu, Z. He, and G. Tang, "Generalized impedance analysis and new sight at damping controls for wind farm connected MMC-HVdc," *IEEE J. Emerg. Sel. Topics Power Electron.*, early access, Aug. 19, 2020, doi: 10.1109/JESTPE.2020.3017896.

[2] C. Wan, J. Zhao, Y. Song, Z. Xu, J. Lin, and Z. Hu, "Photovoltaic and solar power forecasting for smart grid energy management," *CSEE J. Power Energy Syst.*, vol. 1, no. 4, pp. 38–46, Dec. 2015.

[3] A. Dekka, B. Wu, R. L. Fuentes, M. Perez, and N. R. Zargari, "Evolution of topologies, modeling, control schemes, and applications of modular multilevel converters," *IEEE J. Emerg. Sel. Topics Power Electron.*, vol. 5, no. 4, pp. 1631–1656, Dec. 2017.

[4] M. Schroeder and J. Jaeger, "Advanced energy flow control concept of an MMC for unrestricted operation as a multiport device," *IEEE Trans. Power Electron.*, vol. 34, no. 11, pp. 11496–11512, Nov. 2019.

[5] S. Cui, J. Hu, and R. W. De Doncker, "Control and experiment of a TLC-MMC hybrid DC–DC converter for the interconnection of MVDC and HVDC grids," *IEEE Trans. Power Electron.*, vol. 35, no. 3, pp. 2353–2362, Mar. 2020.

[6] T. Huang, H. Xie, B. Wang, T. Cao, and T. Wu, "Study on coordinated control of renewable energy and pump-storage generator connected to MMC-HVDC grid," in *Proc. IEEE Sustain. Power Energy Conf. (iSPEC)*, Beijing, China, Nov. 2019, pp. 225–229.

[7] Z. Ma, F. Gao, X. Gu, N. Li, Q. Wu, X. Wang, and X. Wang, "Multilayer SOH equalization scheme for MMC battery energy storage system," *IEEE Trans. Power Electron.*, vol. 35, no. 12, pp. 13514–13527, Dec. 2020.

[8] M. Hagiwara and H. Akagi, "Experiment and simulation of a modular push–pull PWM converter for a battery energy storage system," *IEEE Trans. Ind. Appl.*, vol. 50, no. 2, pp. 1131–1140, Mar. 2014.

[9] H. Bayat and A. Yazdani, "A hybrid MMC-based photovoltaic and battery energy storage system," *IEEE Power Energy Technol. Syst. J.*, vol. 6, no. 1, pp. 32–40, Mar. 2019.
[10] L. Zhang, F. Gao, and N. Li, "Control strategy of MMC battery energy storage system under asymmetrical grid voltage condition," *Proc. Chin. J. Electr. Eng.*, vol. 2, no. 2, pp. 76–83, Dec. 2016.
[11] L. Zhang, Y. Tang, S. Yang, and F. Gao, "Decoupled power control for a modular-multilevel-converter-based hybrid AC–DC grid integrated with hybrid energy storage," *IEEE Trans. Ind. Electron.*, vol. 66, no. 4, pp. 2926–2934, Apr. 2019.
[12] F. Gao, X. Gu, Z. Ma, and C. Zhang, "Redistributed pulsewidth modulation of MMC battery energy storage system under submodule fault condition," *IEEE Trans. Power Electron.*, vol. 35, no. 3, pp. 2284–2294, Mar. 2020.
[13] S. Samimi, F. Gruson, P. Delarue, F. Colas, M. M. Belhaouane, and X. Guillaud, "MMC stored energy participation to the DC bus voltage control in an HVDC link," *IEEE Trans. Power Del.*, vol. 31, no. 4, pp. 1710–1718, Aug. 2016.
[14] M. Vasiladiotis and A. Rufer, "Analysis and control of modular multilevel converters with integrated battery energy storage," *IEEE Trans. Power Electron.*, vol. 30, no. 1, pp. 163–175, Jan. 2015.
[15] N. Mukherjee and D. Strickland, "Analysis and comparative study of different converter modes in modular second-life hybrid battery energy storage systems," *IEEE J. Emerg. Sel. Topics Power Electron.*, vol. 4, no. 2, pp. 547–563, Jun. 2016.
[16] F. Gao, L. Zhang, Q. Zhou, M. Chen, T. Xu, and S. Hu, "State-of-charge balancing control strategy of battery energy storage system based on modular multilevel converter," in *Proc. IEEE Energy Convers. Congr. Exp. (ECCE)*, Pittsburgh, PA, USA, Sep. 2014, pp. 2567–2574.
[17] M. Quraan, T. Yeo, and P. Tricoli, "Design and control of modular multilevel converters for battery electric vehicles," *IEEE Trans. Power Electron.*, vol. 31, no. 1, pp. 507–517, Jan. 2016, doi: 10.1109/TPEL.2015.2408435.
[18] J. I. Y. Ota, T. Sato, and H. Akagi, "Enhancement of performance, availability, and flexibility of battery energy storage system based on a modular multilevel cascaded converter (MMCC-SSBC)," *IEEE Trans. Power Electron.*, vol. 31, no. 4, pp. 2791–2800, Apr. 2016.
[19] A. Dekka, B. Wu, V. Yaramasu, R. L. Fuentes, and N. R. Zargari, "Model predictive control of high-power modular multilevel converters—An overview," *IEEE J. Emerg. Sel. Topics Power Electron.*, vol. 7, no. 1, pp. 168–183, Mar. 2019.
[20] S. B. Riar, T. Geyer, and K. U. Madawala, "Model predictive direct current control of modular multilevel converters: Modeling, analysis, and experimental evaluation," *IEEE Trans. Power Electron.*, vol. 30, no. 1, pp. 431–440, Jan. 2015.
[21] M. Vatani, B. Bahrani, M. Saeedifard, and M. Hovd, "Indirect finite control set model redictive control of modular multilevel converters," *IEEE Trans. Smart Grid*, vol. 6, no. 3, pp. 1520–1529, May 2015.
[22] J. Bocker, B. Freudenberg, A. The, and S. Dieckerhoff, "Experimental comparison of model predictive control and cascaded control of the modular multilevel converter," *IEEE Trans. Power Electron.*, vol. 30, no. 1, pp. 422–430, Jan. 2015.
[23] J.-W. Moon, J.-S. Gwon, J.-W. Park, D.-W. Kang, and J.-M. Kim, "Model predictive control with a reduced number of considered states in a modular multilevel converter for HVDC system," *IEEE Trans. Power Del.*, vol. 30, no. 2, pp. 608–617, Apr. 2015.
[24] Y. Jin, Q. Xiao, H. Jia, Y. Mu, Y. Ji, T. Dragieevic, R. Teodorescu, and F. Blaabjerg, "A novel sliding-discrete-control-set modulated model predictive control for modular multilevel converter," *IEEE Access*, vol. 9, pp. 10316–10327, 2021.
[25] Y. Sun, Z. Li, and Z. Zhang, "Hybrid predictive control with simple linear control based circulating current suppression for modular multilevel converters," *CES Trans. Electr. Mach. Syst.*, vol. 3, no. 4, pp. 335–341, Dec. 2019.
[26] H. Pan, J. Zhang, C. Deng, H. Ruan, and S. Ma, "Coordinated control of power and current of MMC-HVDC and circulation suppression in unbalanced power grid," in *Proc. IEEE Energy Convers. Congr. Expo. (ECCE)*, Detroit, MI, USA, Oct. 2020, pp. 3420–3427.

QINGQING YUAN was born in 1987. She received the B.S., M.S., and Ph.D. degrees from the China University of Mining and Technology, China, in 2009, 2011, and 2014, respectively. Since 2014, she has been with the Department of Electrical Engineering, University of Shanghai for Science and Technology, China, where she is currently a Teacher. Her current research interests include motor control and renewable energy generation.

FENGNIAN YANG was born in China, in 1996. He received the B.Eng. degree from the Department of Electrical Engineering, Anhui Institute of Information Technology, China, in 2019. He is currently pursuing the M.Eng. degree with the Electrical Engineering Department, University of Shanghai for Science and Technology (USST). His current research interests include power electronics and renewable energy generation.

AN LI was born in China, in 1995. He received the B.Eng. degree from the Department of Electrical Engineering, University of Shanghai for Science and Technology (USST), Shanghai, China, in 2018, where he is currently pursuing the M.Eng. degree. His current research interests include motor control and renewable energy generation.

TING MA was born in China, in 1998. She received the B.Eng. degree from the Department of Electrical Engineering, University of Shanghai for Science and Technology (USST), Shanghai, China, in 2019, where she is currently pursuing the M.Eng. degree. Her current research interests include multiphase and multilevel converters.